Microscopic Simulation of the Temperature Dependence of Static and Dynamic 1.3-μm Multi-Quantum-Well Laser Performance

Bernd Witzigmann, Mark S. Hybertsen, *Member, IEEE*, C. Lewis Reynolds, Jr., *Member, IEEE*, Gregory L. Belenky, *Senior Member, IEEE*, Leon Shterengas, and Gleb E. Shtengel

***Abstract*—The temperature dependence of the performance of 1.3-μm Fabry–Perot (FP) multiple-quantum-well (MQW) lasers is analyzed using detailed microscopic simulations. Both static and dynamic properties are extracted and compared to measurements. Devices with different profiles of acceptor doping in the active region are studied. The simulation takes into account microscopic carrier transport, quantum mechanical calculation of the optical and electronic quantum well properties, and the solution of the optical mode. The temperature dependence of the Auger coefficients is found to be important and is represented by an activated form. Excellent agreement between measurement and simulation is achieved as a function of both temperature and doping profile for static and dynamic properties of the lasers, threshold current density, and effective differential gain. The simulations show that the static carrier density, and hence the contribution to the optical gain, varies significantly from the quantum wells on the p-side of the active layer to those on the n-side. Furthermore, the modal differential gain and the carrier density modulation also vary. Both effects are a consequence of the carrier dynamics involved in transport through the MQW active layer. Despite the complexity of the dynamic response of the MQW laser, the resonance frequency is determined by an effective differential gain, which we show can be estimated by a gain-weighted average of the local differential gain in each well.**

***Index Terms*—Laser modulation response, laser simulation, laser threshold current, optical gain, semiconductor quantum well laser diode.**

I. Introduction

HIGH-temperature operation of semiconductor lasers at 1.3-μm wavelength is important in order to realize low cost and highly reliable telecommunications transmitter modules. Therefore, understanding the temperature-dependent operation of the laser diode is important for proper design. There has been considerable effort to model the temperature dependence of the threshold current. However, only a few studies are based on a detailed microscopic self-consistent description of the laser [1], [2]. Moreover, the temperature-dependent dynamic characteristics have only been investigated using rate equation models without taking into account the spatial distribution of the carrier densities in the multi-quantum-well (MQW) active layer [3].

The temperature dependence of the laser threshold current, often parameterized by T_0, has been widely discussed. This is especially true for InP-based lasers operating in the telecommunications wavelength range where T_0 values are relatively low, implying an undesirable, strong temperature dependence for the threshold current. Various explanations have relied on the temperature dependence of the Auger recombination process, the material gain, the free-carrier absorption, and leakage processes [1], [2], [4]–[9]. However, in practice, all of these physical processes have an important role in the internal operation of the laser, often with a significant interdependence. For this reason, it has proven difficult to isolate a single cause of the low T_0 in these lasers. Microscopic simulation can help identify the crucial physical processes and elucidate the way they interact. Of course, it is essential that there be sufficient independent experimental data to allow a careful calibration of the parameters and the physical models.

Analysis of the dynamic response of the lasers has tended to focus on engineering of the quantum wells to enhance the material differential gain, e.g., through the use of strain or modulation doping [10], [11]. The temperature dependence of the material gain has also been studied [7], [12]. However, there has never been a quantitative link between these quantum-well calculations and the actual modulation response measured. Only relatively recently have microscopic simulations started to unravel some of the interplay between the carrier transport, carrier capture, carrier cooling, and the final modulation response of the MQW lasers [13], [14]. In view of the inhomogeneous pumping of the wells, due to carrier transport constraints, one may well expect the temperature dependence of the laser modulation efficiency to involve competition between transport effects and the gain supplied by the wells.

In this paper, we use a detailed microscopic simulation to analyze the temperature dependence of threshold current and differential gain of 1.3-μm MQW lasers. The simulations are compared to measurements for devices in which the p-doping distribution in the active region has been intentionally varied, modifying the placement of the p-i junction of the diode. This gives a crucial extra dimension to the comparison between the simulations and the experiments. Overall, we show that the simulator can account for the temperature and doping dependence

Manuscript received May 17, 2002; revised September 19, 2002. The work at the State University of New York at Stony Brook was supported in part by ARO Grant DAAD190010423.

B. Witzigmann is with Agere Systems, Alhambra, CA 91803 USA.

M. S. Hybertsen is with Agere Systems, Murray Hill, NJ 07974 USA.

C. L. Reynolds, Jr., is with Agere Systems, Breinigsville, PA 18031 USA.

G. L. Belenky and L. Shterengas are with the State University of New York at Stony Brook, Stony Brook, NY 11794 USA.

G. E. Shtengel was with Agere Systems, Breinigsville, PA 18031 USA. He is now with Kodeos Communications, South Plainfield, NJ 07080 USA.

Digital Object Identifier 10.1109/JQE.2002.806195

of both the threshold current and the modulation efficiency. This is done with a single, consistent set of parameters for the physical models. We provide a detailed analysis of the factors influencing the modulation response.

The paper is organized as follows. In Section II, the model is outlined briefly. Then, the experiments are described. Section IV deals with the temperature dependence of the static laser performance. In Section V, the analysis of small-signal modulation versus temperature is given. Conclusions appear in Section VI.

II. Microscopic Simulation Model

The *LASER* simulator is based on a general drift–diffusion simulator for bulk electron and hole transport. For the quantum well laser device, the optical mode is determined from the solution of the Helmholtz equation and the population of the mode is described by a photon rate equation for each mode. The bulk electrons and holes are coupled to the carriers bound in the quantum wells by a capture process that acts as a local recombination in the regions near a quantum well. The electronic levels in each well and the optical gain are obtained quantum mechanically from a detailed $k \cdot p$ calculation. All the equations are solved self-consistently at each bias point. Self-heating effects are assumed to be negligible in the temperature range and for the current densities of interest. The details and the methodology for the solution have been presented in earlier publications, e.g., [14], [15].

Calibration of the physical models is quite important. Most of the material parameters and physical model parameters are taken from the literature. We now discuss the parameters that are fixed from the device results. The free-carrier absorption process has been well characterized in bulk material. The most important loss mechanism is due to the holes (intervalence band absorption) with a coefficient of 13 cm^{-1} of loss for 10^{18} cm^{-3} holes [16]. However, the coefficient is not known for the quantum wells. We choose a value of 20 cm^{-1} for 10^{18} holes following earlier, direct measurements of loss as a function of current below threshold [7]. In the present simulations, we assume that these coefficients are independent of temperature over the range of interest. The existing experiments [7], [16] suggest that the intervalence band absorption is only weakly dependent on temperature. If it were characterized by a value of "T_0," then the experiments do not give a single value, although something of order 200 K or larger would be appropriate [16].

It is well known that the Auger process accounts for a significant portion of the current at threshold levels in 1.3-μm InGaAsP-based lasers. For the Auger coefficients, room-temperature values between 1–5 $\times$ 10^{-29} cm^6/s are reported for this wavelength [5], [17]–[19]. Their temperature dependence is an even more controversial issue. Reference [20] reports on a combination of a thresholdless and threshold type processes. They extract an activation energy of 40 meV from their calculations. On the other hand, parameter extractions done from either current measurements or carrier lifetime characterizations suggest activation energies up to 140 [9] and 180 meV [5]. These two values result in Auger coefficients being different by a factor larger than three between 300 K and 400 K. This introduces another considerable uncertainty in the Auger parameter for elevated temperatures. In our calculations, the room-temperature Auger coefficients are chosen to be $C_n + C_p = 4 \times 10^{-29}$ cm^6/s. These give the correct threshold current densities for simulations of different device structures [14], [21]. The activation energy for the Auger process is set to $\Delta E = 60$ meV. This is in the range of the previously reported values.

The parameter for the quantum carrier capture model is chosen to be $\tau = 1$ ps for both holes and electrons. This value fits adequately with the constraints of room temperature device data [22]. The capture model has intrinsic temperature dependence, but the coefficient is held constant. Finally, the simulator does not explicitly represent fast carrier processes in the individual wells such as carrier–carrier scattering or carrier–phonon scattering. Spectral hole burning and carrier heating are known to be fundamental sources of gain compression [13], [23]. We include a phenomenological gain compression coefficient $\varepsilon = 2 \times 10^{-17}$ cm^{-3} in each well. This results in damping of the resonance in the small-signal modulation of the observed magnitude.

In summary, the parameters that were chosen on the basis of laser device data are the quantum well intervalence band absorption, the Auger model, the capture model, and the gain compression model. All other material parameters are standard values from the literature. This gives one consistent set of input parameters that has been used previously to explain static and dynamic properties for 1.3-μm MQW lasers at room temperature. This parameter set and the underlying models are now applied to the calculation of threshold currents and small-signal modulation responses for a range of temperatures from 300 K to 360 K. This covers the critical range of operation for telecommunication applications.

III. Experiment

A detailed description of the devices and the measurement techniques is given in [21], [24], and [25]. The InGaAsP–InP devices were grown by low pressure metalorganic chemical vapor deposition (MOCVD) on InP substrates. The active region consists of nine quantum wells (70 Å) with compressively strained wells ($\sim$1%) designed for operation near 1.3 μm. The separate confinement layers (500 Å) and the barriers (100 Å) have the same InGaAsP material composition ($\lambda = 1.15$ μm). Two classes of devices were fabricated. Broad area lasers with a contact width of 100 μm were used for the T_0 characterization. This minimizes the impact of lateral leakage currents out of the active layers. The dynamic characterization used standard capped-mesa-buried-heterostructure (CMBH) lasers with a mesa width of about 1 μm. The relaxation oscillation frequency was determined from relative intensity noise spectra (RIN). The spectra were detected with a high-speed InGaAs p-i-n photodetector and a low noise preamplifier. The doping profiles of all of the devices were obtained using the secondary ion mass spectrometry (SIMS) characterization.

IV. Static Laser Performance: Characteristic Temperature T_0

Devices with two different doping profiles have been used. For the one set, indicated by undoped, the p++-i-junction is lo-

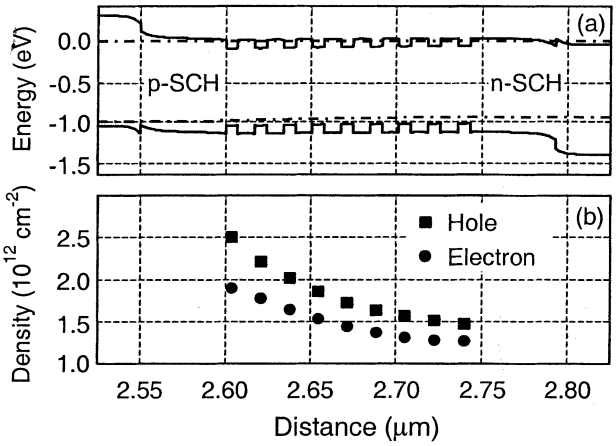

Fig. 1. (a) Band diagram (solid lines) and quasi-Fermi levels (dashed-dotted lines) for an undoped active broad area laser at threshold current. (b) Quantum-well electron and hole density in each well.

cated at the interface between the separate confinement region and p-cladding. This ensures low electron leakage currents into the p-cladding due to the additional electrostatic barrier [6] (see Fig. 1). The simulations show that at threshold bias level, the heterobarrier electron leakage into the p-cladding for the doped device is smaller than 1% for all temperatures considered. This agrees well with results for special devices designed for direct measurement of the heterobarrier leakage [26]. For the second set, designated low doped, the p-doping extends through the p-SCH layer and penetrates three of the nine wells with a dopant concentration of 1.5×10^{18} cm^{-3}.

In general, the bulk carrier transport through the MQW active region involves the competition between the drift (responding to the local quasi-Fermi level) and the capture process, acting as a local recombination process. Further, the accumulation of carriers in the wells locally distorts the band profile through the electrostatic potential. Fig. 1 illustrates the resulting self consistent band profile in the active layer for the undoped example. The quantum wells for electrons are relatively shallow, with low capacity for stored carriers resulting in quasi-Fermi levels that ride near the top of the well. The effective mobility for transport of bulk electrons across this region is relatively high and the quasi-Fermi level for the bulk electrons is relatively flat. However, the quantum wells for holes are deeper and they have a capacity for carriers substantially larger than the carrier density required for the gain. The hole quasi-Fermi levels fall well into the gap. The transport of holes through the active region is largely sequential capture and reemission from each well in turn [22]. This leads to a low effective mobility for the bulk holes and the evident variation in the bulk hole quasi-Fermi level across the active region. Thus, the dynamics of carrier capture into the quantum wells cause a carrier accumulation at the p-side of the quantum well stack, as illustrated in Fig. 1. This results in different well pumping levels, which is taken into account by the simulation and transforms into a gain variation by a factor of five between the n-side well and the p-side well in this example.

It is difficult to probe the inhomogeneous carrier population in the wells directly, although some indirect experimental evidence exists [27]. However, the net gain spectrum is the composite of the contributions from the nine individual wells, which

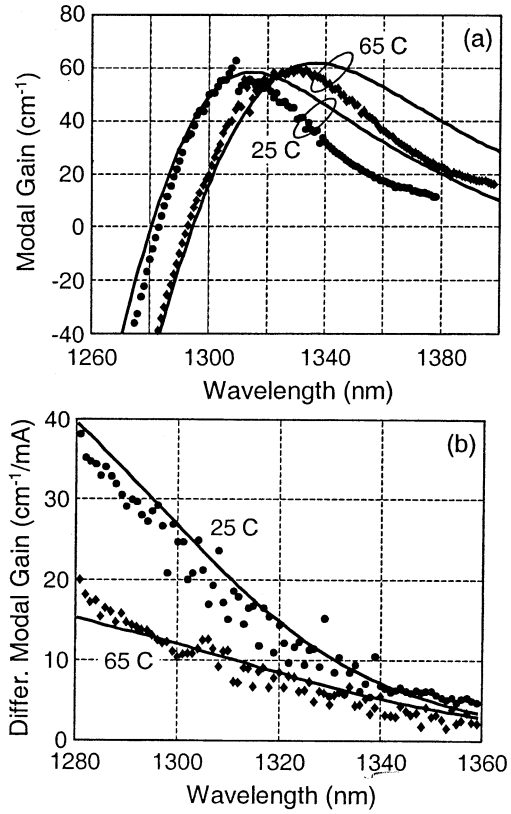

Fig. 2. (a) Simulated (line) and measured (dots) modal gain spectra near the threshold current for two different temperatures $T = 25$ °C and $T = 65$ °C. Data and simulation taken for a buried heterostructure laser in the low-doped case. (b) Differential modal gain taken as a finite difference with respect to current below threshold. Simulation and experiment as in (a).

can be quite different [12]. The net gain spectrum has been measured for CMBH devices with different doping profiles and at different temperatures [7]. The transparency wavelength has also been measured directly [7]. This is the wavelength at which the material gain due to interband transitions is exactly zero. Combined with the net gain measurement, one has the total loss at the transparency wavelength. The mirror loss can be estimated for these devices since they have cleaved facets. We assume that the intervalence band absorption scales as λ^3 [16] to convert the measured net gain spectra into modal gain spectra. Spectra measured at two temperatures for a device with low doping in the active biased to near (but not at) threshold are plotted in Fig. 2(a). The corresponding simulated spectra are shown for comparison. The simulation accounts for the overall spectral shape, especially between the transparency wavelength and the peak of the gain, which is most significant for practical laser operation. The simulated spectra are broader on the long wavelength side, probably due to the neglect of vertex corrections (essentially excitonic correlations) in the gain calculation [28], [29]. Otherwise, the simulation accounts for the change in spectral width with temperature and the shift of the transparency wavelength.

The differential modal gain has been computed as a finite difference for a current just below threshold. The resulting spectra are plotted in Fig. 2(b), showing a comparison of simulation and experiment at the same two temperatures. The simulation has been scaled by a factor of 1.8, as discussed below. From

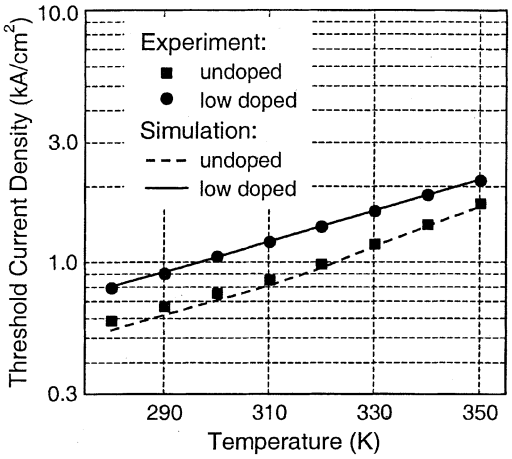

Fig. 3. Threshold current density versus temperature for InGaAsP 1.3-μm broad-area lasers without and with partial doped active region. The lines are simulation results and the solid symbols are measurements.

Fig. 2(b), one sees that the simulations accurately account for the change in the differential gain with temperature.

The additional carriers in the active region due to doping or due to higher temperature contribute to a higher nonradiative recombination and to increased free carrier (intervalence band) absorption. Thus, the modal loss increases with current up to threshold and the total modal loss that must be overcome to achieve threshold goes up both with increased doping and with increased temperature. The simulations reproduce this trend. However, with the assumption of a temperature independent free carrier absorption coefficient, the quantitative change between 25 °C and 65 °C is smaller than measured (2 cm^{-1} versus 8 cm^{-1} for the low-doped devices). We noted the experimental uncertainty on the temperature dependence of the free-carrier absorption coefficient. This discrepancy between the simulated and measured temperature dependence of the loss may be evidence of temperature dependent free carrier absorption. However, the details of the loss mechanisms should be investigated further.

Fig. 3 shows the measured and simulated threshold currents versus temperature for the two devices. For both cases, the agreement of threshold current is very good for the entire temperature range. In [21], it has already been shown that the simulation can explain the threshold current variation versus p-doping setback at room temperature. Here, we find a good account of the temperature dependence. For the low-doped case, the simulation gives a characteristic temperature of $T_0 = 70$ K; the measurements result in $T_0 = 71$ K. For the undoped case, the slope of the curves shown increases with temperature, indicating a dropping T_0. Fitting linear functions for the low temperature and the high temperature regime, it is possible to extract two characteristic temperatures. The intersection point is often denoted by a critical temperature T_C. As shown in the summary in Table I, the simulation agrees well with the experiments.

Different interpretations of the origin of T_C have been given in literature. In [1], it was indicated that this could be due to increased nonradiative recombination in the p-SCH. Other publications claim this to be due to the onset of leakage currents

TABLE I
SUMMARY OF THE T_0 DATA OBTAINED BY THE MICROSCOPIC SIMULATION AND THE MEASUREMENTS FOR THE TWO DIFFERENT DEVICE TYPES

	T_0 (K)	
	$T<T_c$	$T>T_c$
InGaAsP (doped)		
Experiment	71	71
Simulation	70	70
InGaAsP (undoped)		
Experiment	79	53
Simulation	71	54

[4]. In our measurements, we observe a decrease of T_0 for the undoped case, but not for the low-doped case. From the simulations, the leakage currents into the p-cladding are small at threshold for both devices and cannot account for this effect, which has also been confirmed experimentally in [24]. An analysis of the different current components entering the calculation of T_0 shows that the critical temperature is caused by a transition from the regime where the radiative current dominates to the Auger current dominated regime. In the doped case, the presence of a background hole density increases the total carrier density. This contributes to a higher relative Auger component in the threshold current at a fixed temperature. The transition to the Auger dominated regime is therefore taking place at lower temperatures, and a critical temperature does not occur in the displayed temperature range. The direct comparison shows that doping in the active region increases T_0 in the high temperature regime. The ionized acceptors of the doped active modify the shape of the energy bands of the quantum wells. This results in a larger effective well depth for electrons, which is beneficial for high temperature operation.

When the simulations are applied to the CMBH devices, which have been fabricated from the same active layer design as the wide area devices, we find that the simulated threshold current (4 mA) is substantially lower than the measured threshold current (7 mA) at room temperature. At the same time, the simulated T_0 is the same as that measured for these devices. Part of the difference in the magnitude of the threshold current may trace to uncertainty concerning the exact width of the active layer. However, we believe that most of the difference arises from extra lateral current near the edge of the active region in the CMBH devices. This has recently been measured directly for similar devices [30]. The precise mechanism of this lateral leakage is not known, but it has been shown to clamp at threshold. For the present discussion, there are two significant points. First, this justifies the correction factor applied to the static differential gain spectra in Fig. 2(b). Second, because the leakage clamps above threshold, it has no impact on the study of the modulation response.

V. SMALL-SIGNAL MODULATION

In this section, the focus is on the modulation efficiency of MQW lasers and its temperature dependence. The modulation efficiency determines the optical resonance frequency of the device due to electrical modulation at the contacts. Parasitic elements of the diode are not considered in this simulation. Therefore, the modulation efficiency is represented by the effective differential gain, an intrinsic measure, for ease of comparison

to experiment. Experimental values are extracted from the measured resonance frequency. Fundamentally, the effective differential gain is determined both by the intrinsic differential gain of the quantum wells and the carrier dynamics of the entire device structure [31], [32]. In the full simulations, the small-signal response is analyzed following the same procedures used for the experimental data.

Experiments have been conducted with CMBH devices described in the previous section, with two different doping concentrations in the active region. The device indicated as *low doped* has an acceptor concentration of 1.5×10^{18} cm^{-3} up to the third quantum well from the p-side of the MQW stack. The device indicated as *high doped* contains an acceptor concentration of 2.5×10^{18} cm^{-3} in eight of the nine wells.

We start by setting up the framework for the discussion. The rate equation for the photon density S with a MQW configuration is

$$\frac{dS}{dt} = v_g \left(\sum_m G_m - L \right) S + \beta R_{sp} \tag{1}$$

where G_m are the mode gain contributions from each well, L is the optical loss, v_g is the group velocity, and $\beta R_{\rm sp}$ is the spontaneous emission coupled into the mode of interest. In the microscopic simulator, this equation is coupled to the full solution of the carrier transport and the bound carriers in each of the wells that provides the gain G_m. Standard small-signal analysis is performed with $S = S_0 + ds/dV^* dV\, e^{i\omega t}$ and $G_m = G_{m0} + dg_m/dV^* dV\, e^{i\omega t}$. Inserting S and G_m and solving for ds gives (where G_0 is the total steady-state gain

$$\frac{ds}{dV} = \frac{S_0}{i\omega - v_g(G_0 - L)} \sum_m \frac{dg_m}{dV}. \tag{2}$$

The microscopic simulation contains all the values at the right-hand side, with the gain modulation

$$\frac{dg_m}{dV} = \frac{dg_m}{dn}\frac{dn_m}{dV} + \frac{dg_m}{dp}\frac{dp_m}{dV} \tag{3}$$

where the differential modal gains dg_m/dn and dg_m/dp are the static differential gains and the carrier modulations dn_m/dV and dp_m/dV are the complex carrier density differentials in the quantum wells due to an external voltage modulation dV. Thus, the modulation of the gain is divided into two distinct contributions. The static differential gain in each well is determined by the quantum-well properties and the static carrier distribution among the quantum wells in the active layer of the device. The carrier modulations depend on the details of the dynamical carrier transport.

Analytical results can be obtained from a rate equation approach. A commonly employed model includes both an above barrier carrier population and a bound carrier population coupled by capture and reemission time constants. The analysis of this model results in a widely used approximate expression for the modulation response [33]

$$M(\omega) = \frac{1}{1 + i\omega\tau_s} \frac{A}{\omega_r^2 - \omega^2 + i\omega\gamma} \tag{4}$$

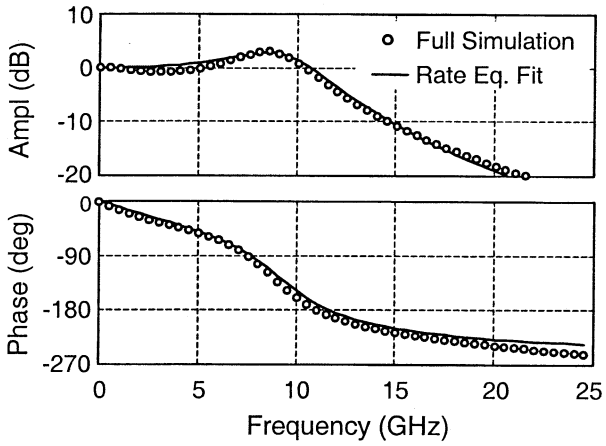

Fig. 4. Small-signal optical modulation response for a nine-quantum-well InGaAsP laser, amplitude (upper panel), and phase (lower panel). The full microscopic simulation (open circles) and a fit to the rate equation model (solid line) are shown. The operation bias is 45 mA above threshold.

where τ_s is an effective carrier transport time and γ is the damping rate for which an explicit expression can be derived. The expression for the resonance frequency reads

$$\omega_r^2 = \frac{v_g \Gamma \eta_i}{qV} \frac{dG^*}{dN}(I - I_{th}) \tag{5}$$

where $I - I_{\rm th}$ is the overdrive current above threshold level, Γ is the optical confinement factor, V the active volume, η_i the internal efficiency, and dG^*/dN is the effective differential gain. The effective differential gain depends on the details of the dynamics in the carrier rate equations. This result suggests that, despite the extra complexity of the carrier dynamics, the form of the resonance response of the laser may be expected to follow the standard form of a damped oscillator, only with the addition of an extra rolloff. It also reinforces the point made above: the resonance frequency is controlled by an effective differential gain that includes the influence of transport.

Of course, the full microscopic simulation includes all the dynamics of the carriers, including the effects of multiple wells. Fig. 4 shows a comparison of the modulation response obtained from the microscopic simulation and a fit using (4). The quality of the fit is satisfactory, and the transport factor τ_s gives a good description of the additional linear drop in the phase due to carrier dynamics. In the low-frequency regime (around 5 GHz in Fig. 4), the microscopic simulation shows some rolloff that is not well reproduced by the fit. We use this fitting procedure to obtain the simulated resonance frequency.

Fig. 5 shows the resonance frequencies versus overdrive current from the microscopic simulation. In comparison, the resonance frequency extracted from the RIN measurements is also shown. The data is shown for the low-doped device at room temperature. Excellent agreement is obtained. The slope of the curve in Fig. 5 gives the effective differential gain dG^*/dN. We use the same constants in (5) for analysis of the simulation and the experiment ($\eta_i = 1$, $n_g = 3.7$ and $\Gamma = 0.01$ per 70 Å well). In the analysis of the simulated modulation response across the range of device doping and temperature considered, the extraction of the differential gain is based on the overdrive

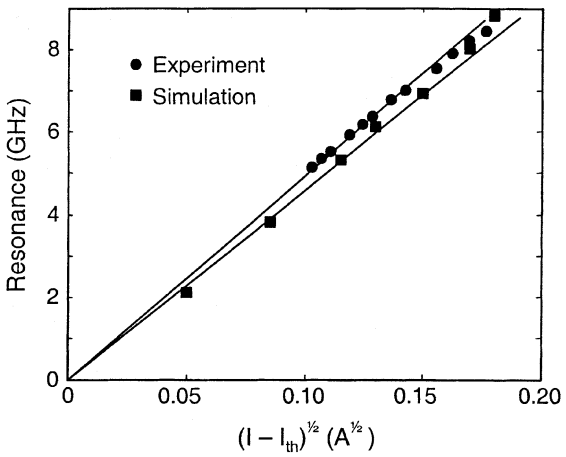

Fig. 5. Resonance frequency versus square root of the overdrive current for the low doped case. Compared are simulated small-signal results and measured RIN results at room temperature.

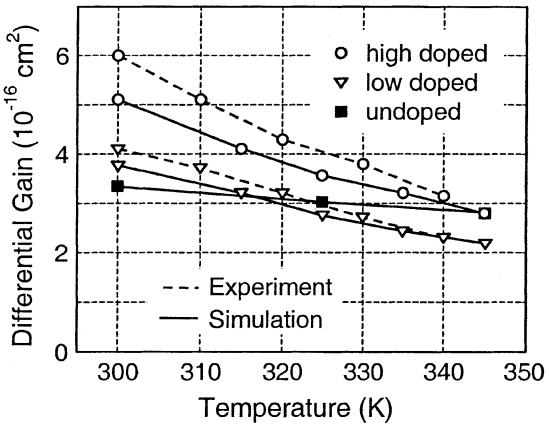

Fig. 6. Differential gain versus temperature for 1.3-μm MQW lasers with different p-doping in the active region. Dashed lines are measured data. Solid lines were obtained from the simulations.

current range of 10 to 40 mA, where the quality of the fits to (4) is best.

This procedure has been applied to study the doping and temperature dependence of the modulation response. Fig. 6 shows the effective differential gain versus temperature. The simulation includes devices with three different doping densities in the active region. Measurements have been taken from [25] and the devices are either low doped or high doped. The overall agreement between the simulations and the experiments is excellent. We stress that no parameter is fitted to give the modulation efficiency. The agreement of the simulation to the experiments is the result of the interplay of the physical models in the simulator that have been independently calibrated as described above.

Introducing doping, the modulation efficiency at room temperature is increased (see also e.g., [11], [34]). At the same time, the temperature sensitivity of the effective differential gain is also increased. The high-doped case shows a decrease of 45% over the temperature range between 300 K and 340 K. The low-doped case is less sensitive. The simulations show a decrease of about 15% for the undoped case.

The qualitative trends can be understood from the basics of gain in quantum wells. As discussed in [25], the differential gain is controlled by the electron population in the wells. This follows from the ratio of the electron to the hole mass. Even for compressively strained quantum wells, the hole mass is still substantially larger. Introduction of p-type doping in the quantum well allows for achieving the threshold condition with a lower electron population. This gives a larger differential gain. However, at the same time, it also leads to a larger temperature coefficient.

This qualitative explanation only considers the material differential gain in the quantum wells. It is interesting to understand the impact of the carrier dynamics. As we stressed in discussing (3), the effective differential gain also depends on the details of the carrier transport to give the distribution of carrier density modulation. The carrier densities are coupled by both interwell carrier exchange coming from capture and re-emission of carriers and the coupling of the well carrier populations to a single photon population via the stimulated emission. This is a nontrivial process.

The first impact of the carrier dynamics is to cause an inhomogeneous distribution of the carriers in the different wells of a MQW stack (Fig. 1). Therefore, each well contributes a different amount of gain to the total gain and linear scaling rules do not apply in general. Differential gain in a quantum well depends both on the level of inversion and on the wavelength detuning. This leads to an inhomogeneous distribution of the static material differential gain dg_m/dn and dg_m/dp in each well of the MQW laser. These steady-state effects are illustrated for the devices biased to about 45 mA above threshold. The modal gain is plotted for each well in Fig. 7, along with the modal differential gain for each well. The impact of doping on the modal gain is relatively small. The spread from p-side (well number 1) to n-side is about the same. However, the doping has a substantial impact on the differential gain. This effect follows from the qualitative argument given above.

Now we turn to the carrier modulation, which is also shown in Fig. 7. The values are taken at the resonance frequency for a voltage modulation of 3 mV at the contact. In general, the finite transport time between the wells additionally adds a phase to the modulation, and dp_m/dV and dn_m/dV are complex quantities. However, at resonance, the well carrier modulation is strongly coupled to the photon population, and therefore the phase difference between the wells is nearly zero and can be ignored [35]. The wells at the p-side (well 1) have the highest modulation values. This is intuitively reasonable and consistent with the static carrier distribution (Fig. 1). Furthermore, the distribution is not markedly influenced by the doping. This may be surprising at first, since increased doping is associated with increased conductivity for bulk semiconductors. However, the net effect of the doping in the quantum well regions is to spill the extra holes into the wells leaving ionized acceptors in the barriers. The impact on the transport only comes through some alteration in the band profile, and hence the capture and emission processes. In Fig. 7, there is a slight improvement in the modulation of the n-side wells with increased doping.

The effective differential gain combines the carrier modulation with the local differential gain well by well as in (3). As can

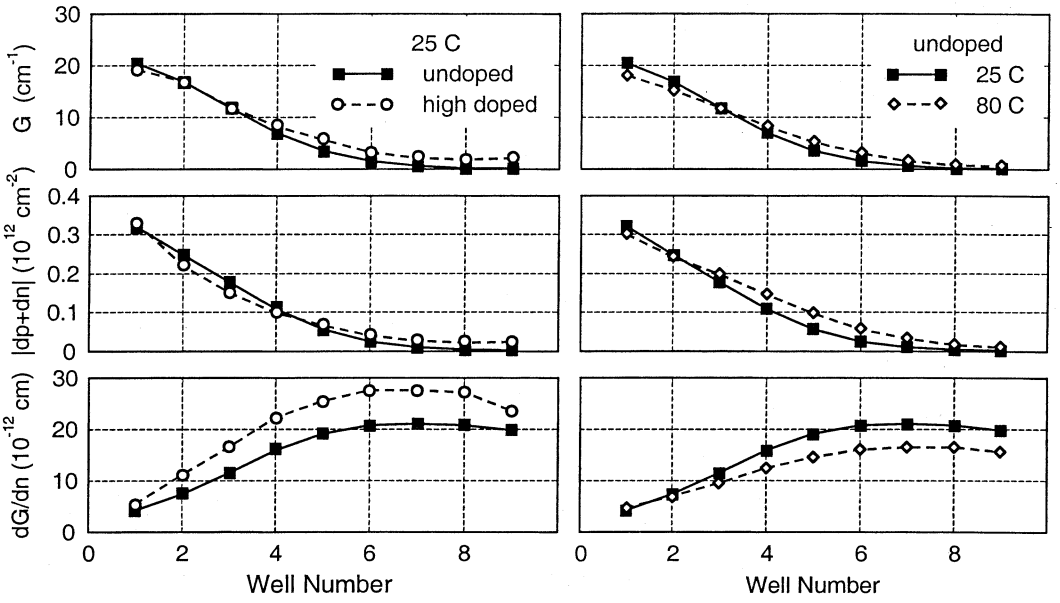

Fig. 7. Comparison of modal gain, carrier modulation, and differential modal gain in each of the nine quantum wells in a MQW laser, biased 45-mA above threshold. (a) Compares an undoped active layer device to one with high p-doping, as described in the text at a fixed temperature of 25 °C. (b) The same undoped device at two different temperatures. The lines are guides for the eye.

be seen from Fig. 7, the wells with the largest carrier modulations also possess the lowest static differential gains. As a consequence, the observed effective differential gain is smaller than what would be estimated by looking at an average quantum well and ignoring the transport effects. Increasing the doping mostly increases the static differential gain. There may also be a small increase due to more effective modulation of the n-side wells.

At elevated temperatures, the carrier modulation differentials dn_m/dV and dp_m/dV increase and the ability to modulate the n-side wells improves slightly (Fig. 7). This is reasonable as one would expect the capture and emission processes that control the hole modulation to be somewhat faster. This increase is similar for the undoped and the doped active device. On the other hand, the static differential gain decreases with higher temperatures following the qualitative discussion above. This is illustrated in Fig. 7 for the undoped case. These two effects compete. For the undoped device, the net result is a relatively weak temperature dependence of the effective differential gain (Fig. 6). However, with increasing doping, the decrease in the static differential gain is larger and dominates over the increasing carrier modulation.

As we emphasized, the modulation of the photons in the laser depends on the differential gain in the individual wells (generally different) and the modulation of the carrier populations bound in each individual well, generally different for each well and complex due to the carrier dynamics. If we focus on the resonance frequency, it is possible to get a simplified view. The electron and hole modulations are largely in phase [35]. In the present lasers, this traces to the relatively shallow electron wells, so the electrons can easily follow the holes. We then write a set of rate equations for the composite bound carriers in the MQW case, as follows:

$$\frac{dn_m}{dt} = \frac{I_m}{qV_m} - R_{\rm Aug} - R_{\rm spon} - v_g g_m S \tag{6}$$

where n_m is the bound density of well m, I_m is the current into this well, g_m is the material gain in this well, V_m is the well volume, the $R_{\rm Aug}$ and $R_{\rm spon}$ describes the recombination in the well, and the other symbols have their usual meaning. In principle, this is no simplification since the modulation of the current into each well remains unknown without a detailed simulation. However, we have also noted that at the resonance frequency, the bound carriers are modulated in phase, to a good approximation, and 90° out of phase to the photons, as expected for a resonance [35]. This was also observed in some previous simulations [32]. Therefore, it is reasonable to examine the small-signal expansion of the (1) and (6) and look for the condition for undriven oscillations

$$j\omega_0 = \sum_m \gamma_m^s - \sum_m \frac{\omega_m^2}{j\omega_0 + \gamma_m^n} \tag{7}$$

where we have defined

$$\gamma_m^s = v_g S \Gamma_m \frac{dg_m}{dS} \tag{8}$$

$$\gamma_m^n = \frac{1}{\tau_m} + v_g S \frac{dg_m}{dn_m} \tag{9}$$

$$\omega_m^2 = v_g^2 S \Gamma_m \left(g_m + S \frac{dg_m}{dS} \right) \frac{dg_m}{dn_m} \tag{10}$$

and the complex response frequency sought is ω_0. The possibility of gain compression has been included. In general, the response frequency will be a zero of the $N_{QW}+1$-order polynomial implicit in (7). However, a reasonable approximation follows under the assumption that $\gamma_m^n < \omega_0$

$$\omega_0^2 \cong j\omega_0 \sum_m \left(\frac{\omega_m^2}{\omega_0^2} \gamma_m^n - \gamma_m^s \right) + \sum_m \omega_m^2 \equiv j\omega_0 \Gamma + \omega_r^2 \tag{11}$$

where, in the last identity, the conventional terminology from the usual rate equation expressions has been used. One can verify that the approximation used to arrive at (11), in the limit of a single carrier population, reduces to the usual expressions provided that the damping Γ is not too large relative to the resonance frequency ω_r. This condition just comes from the substitution of ω_r for ω_0 in the damping portion of (11). There is also a small term in the usual expression for ω_r^2 related to the dg/dS which is lost.

Now we can get simplified expressions for the resonance frequency in terms of the well-by-well properties

$$\omega_r^2 \cong v_g^2 S \sum_m \Gamma_m g_m \frac{dg_m}{dn_m} \equiv v_g^2 S G \frac{dg^*}{dn} \tag{12}$$

where G is the total modal gain and we introduce an effective differential gain dg^*/dn, which is just the gain-averaged local differential gain

$$\frac{dg^*}{dn} = \sum_m \Gamma_m g_m \frac{dg_m}{dn_m} \Bigg/ \sum_m \Gamma_m \, g_m. \tag{13}$$

An expression for the damping can also be derived. However, the present analysis explicitly ignored the drive currents into each well, which from the simulations we know to have a nontrivial phase as a function of frequency away from the resonance frequency. This is found in the microscopic simulations through the phase relations among the dn_i and dp_i, which vary substantially with frequency, except close to the resonance frequency. This will contribute to the shape of the resonance and hence the damping constant.

Equation (13) gives a simplified expression for the effective differential gain, which takes into account the inhomogeneous carrier populations among the wells. It shows that the resonance frequency does not depend on all of the details of the complex carrier dynamics in the MQW active region, just the steady state distribution of the carriers at the operating point. We have examined the predictions of (13) and find that it gives the qualitative trends reported in Fig. 6 from the full simulation. Quantitatively, it predicts the effective differential gain within 10%–20%.

VI. Conclusion

We have presented a systematic investigation of the temperature dependence of the static and dynamic properties of 1.3-μm InGaAsP MQW lasers. The microscopic simulations account for both the background doping and the temperature dependence of the threshold current density and the modulation efficiency. In each case, the simulation result comes from the nontrivial interplay of more than one physical effect. From the details of the simulations, we can develop some insight into the fundamental device operation.

The temperature dependence of the threshold current traces both to the reduction in the material gain as well as the increase in the Auger recombination. The increase in loss due to higher carrier density in the active region plays a secondary role. The critical temperature observed near 50 °C in the undoped device indicates a crossover to Auger-dominated recombination. Leakage currents from the p-SCH into the barriers have a negligible impact on the threshold current up to temperatures of 85 °C in these devices. Increased p-doping in the active region increases the absolute threshold current, but also improves the characteristic temperature at high operation temperatures. This traces to the selfconsistent change in the band profile near the wells that improves electron confinement. The higher bound carrier densities in the doped region also lead to Auger-dominated recombination at a lower temperature. No critical temperature is observed in the temperature window studied.

The modulation efficiency of the MQW laser is strongly influenced by the carrier transport through the active region. First, the carrier dynamics lead to a steady state distribution of the bound carriers that is nonuniform among the wells. In the present devices, the holes are concentrated in the wells on the p-side of the active layer. As a consequence, the first three wells supply most (approximately 75%) of the modal gain. However, as a direct consequence, these wells have a lower differential gain. This follows from the fundamentals of quantum well gain. Second, the carrier dynamics leads to a nonuniform carrier modulation when the device bias is modulated. The modulation response roughly follows the steady state carrier distribution, an intuitively reasonable result. Combined with the first point, the wells with the largest carrier modulation (and the largest contribution to the modal gain) have the smallest differential gain. This leads to a lower overall modulation efficiency than would be naively expected if the quantum wells were uniformly populated. The impact of p-doping in the active region, or changes in temperature, largely derive from the fundamentals of quantum-well gain. However, the final quantitative results also depend on small doping or temperature induced changes in the MQW transport. Finally, although the full modulation response depends on the details of the carrier modulation as a function of frequency [(2) and (3)], we have shown that the effective differential gain that controls the resonance frequency can be estimated from a simple gain-weighted average of the differential gain in each well (13).

So far, we have not discussed a direct signature of the carrier dynamics in the modulation response. The rate equation models suggest the possibility of substantial low-frequency rolloff, for example, directly tied to an effective transport time scale (carrier diffusion or carrier capture related depending on details of the active layer). In the present devices, we do not observe any such dramatic signatures. There are, however, more subtle effects, such as a doping dependence of the damping factor and the linear component in the phase of the modulation response. These will be the subjects of future investigation.

References

[1] S. Seki, H. Oohashi, H. Sugiura, T. Hirono, and K. Yokoyama, "Study on the dominant mechanisms for the temperature sensitivity of threshold current in 1.3 μm InP-based strained-layer quantum-well lasers," *IEEE J. Quantum Electron.*, vol. 32, pp. 1478–1486, 1996.

[2] J. Piprek, P. Abraham, and J. E. Bowers, "Self-consistent analysis of high-temperature effects on strained-layer multiquantum-well InGaAsP–InP lasers," *IEEE J. Quantum Electron.*, vol. 36, pp. 366–374, 2000.

[3] T. Keating, X. Jin, S. L. Chuang, and K. Hess, "Temperature dependence of electrical and optical modulation responses of quantum well lasers," *IEEE J. Quantum Electron.*, vol. 35, pp. 1526–1534, 1999.

[4] A. A. Bernussi, H. Temokin, D. L. Coblentz, and R. A. Logan, "Effect of barrier recombination on the high temperature performance of quaternary multiquantum well lasers," *Appl. Phys. Lett.*, vol. 66, pp. 67–69, 1995.
[5] J. M. Pikal, C. S. Menoni, P. Thiagarajan, G. Y. Robinson, and H. Temkin, "Temperature dependence of intrinsic recombination coefficients in 1.3 μm InAsP/InP quantum-well semiconductor lasers," *Appl. Phys. Lett.*, vol. 76, pp. 2659–2661, 2000.
[6] R. F. Kazarinov and M. R. Pinto, "Carrier transport in laser heterostructures," *IEEE J. of Quantum Electron.*, vol. 30, pp. 49–53, 1994.
[7] D. A. Ackerman, G. E. Shtengel, M. S. Hybertsen, P. A. Morton, R. F. Kazarinov, T. Tanbun-Ek, and R. A. Logan, "Analysis of gain in determining T_0 in 1.3 μm semiconductor lasers," *IEEE J. Select. Topics Quantum Electron.*, vol. 1, pp. 250–263, 1995.
[8] N. K. Dutta and R. J. Nelson, "The case for auger recombination in $In_{1-x}Ga_xAs_yP_{1-y}$," *J. Appl. Phys.*, vol. 53, pp. 74–92, 1982.
[9] A. F. Phillips, S. J. Sweeney, A. R. Adams, and P. J. A. Thijs, "The temperature dependence of 1.3- and 1.5-μm compressively strained InGaAs(P) MQW semiconductor lasers," *IEEE J. Select. Topics Quantum Electron.*, vol. 5, pp. 401–412, 1999.
[10] M. Nido, K. Naniwae, J. Shimizu, S. Murata, and A. Suzuki, "Analysis of differential gain in InGaAs–InGaAsP compressive and tensile strained quantum-well lasers and its application for estimation of high-speed modulation limit," *IEEE J. Quantum Electron.*, vol. 29, pp. 885–889, 1993.
[11] K. Uomi, "Modulation-doped multi-quantum well (MD-MQW) lasers. I. Theory," *Jpn. J. Appl. Phys.*, vol. 29, pp. 81–87, 1990.
[12] S. Seki, K. Yokoyama, and P. Sotirelis, "Theoretical analysis of high-temperature characteristics of 1.3-μm InP-based quantum-well lasers," *IEEE J. Select. Topics Quantum Electron.*, vol. 1, pp. 264–274, 1995.
[13] M. Grupen and K. Hess, "Simulation of carrier transport and nonlinearities in quantum-well laser diodes," *IEEE J. Quantum Electron.*, vol. 34, pp. 120–140, 1998.
[14] M. A. Alam, M. S. Hybertsen, R. K. Smith, and G. A. Baraff, "Simulation of semiconductor quantum well lasers," *IEEE Trans. Electron Devices*, vol. 47, pp. 1917–1925, 2000.
[15] M. S. Hybertsen, B. Witzigmann, M. A. Alam, and R. K. Smith, "Role of carrier capture in microscopic simulation of multi-quantum-well semiconductor laser diodes," *J. Comput. Electron.*, vol. 1, pp. 113–118, 2002.
[16] C. H. Henry, R. A. Logan, F. R. Merritt, and J. P. Luongo, "The effect of intervalence band absorption on the thermal behavior of InGaAsP lasers," *IEEE J. Quantum Electron.*, vol. QE-19, pp. 947–952, 1983.
[17] C. H. Henry, B. F. Levine, R. A. Logan, and C. G. Bethea, "Minority carrier lifetime and luminescence efficiency of 1.3 mm InGaAsP–InP double heterostructure layers," *IEEE J. Quantum Electron.*, vol. QE-19, pp. 905–912, 1983.
[18] A. Mozer, K. M. Romanek, O. Hildebrand, W. Schmid, and M. H. Pilkuhn, "Losses in GaInAs(P)/InP and GaAlSb(As)/GaSb Lasers—The influence of the split-off valence band," *IEEE J. Quantum Electron.*, vol. QE-19, pp. 913–916, 1983.
[19] G. E. Shtengel, D. A. Ackerman, P. A. Morton, E. J. Flynn, and M. S. Hybertsen, "Impedance-corrected carrier lifetime measurements in semiconductor lasers," *Appl. Phys. Lett.*, vol. 67, pp. 1506–1508, 1995.
[20] N. A. Gun'ko, A. S. Polkovnikov, and G. G. Zegrya, "A numerical calculation of auger recombination coefficients for InGaAsP/InP quantum well heterostructures," *Semiconductors*, vol. 34, pp. 448–452, 2000. [Online] Available: http://www.ioffe.rssi.ru/SVA/NSM.
[21] M. S. Hybertsen, M. A. Alam, G. E. Shtengel, G. L. Belenky, C. L. Reynolds, Jr., D. V. Donetsky, R. K. Smith, G. A. Baraff, R. F. Kazarinov, J. D. Wynn, and L. E. Smith, "Role of p-doping profile in InGaAsP multi-quantum well lasers: Comparison of simulation and experiment," *Proc. SPIE*, vol. 3625, pp. 524–534, 1999.
[22] M. S. Hybertsen, M. A. Alam, R. K. Smith, G. E. Shtengel, C. L. Reynolds, Jr., and G. L. Belenky, "Simulation of carrier dynamics in multi-quantum well lasers," *Proc. SPIE*, vol. 3944, pp. 486–491, 2000.
[23] M. A. Alam and M. S. Lundstrom, "Effects of carrier heating on laser dynamics—A Monte Carlo study," *IEEE J. Quantum Electron.*, vol. 33, pp. 2209–2220, 1997.
[24] G. L. Belenky, C. L. Reynolds, Jr., D. V. Donetsky, G. E. Shtengel, M. S. Hybertsen, M. A. Alam, G. A. Baraff, R. K. Smith, R. F. Kazarinov, J. Winn, and L. E. Smith, "Role of p-doping profile and regrowth on the static characteristics of 1.3 μm MQW InGaAsP–InP lasers: Experiment and modeling," *IEEE J. Quantum Electron.*, vol. 35, pp. 1515–1519, 1999.
[25] G. L. Belenky, C. L. Reynolds, Jr., L. Shterengas, M. S. Hybertsen, D. V. Donetsky, G. E. Shtengel, and S. Luryi, "Effect of p-doping on the temperature dependence of differential gain in FP and DFB 1.3 μm InGaAsP–InP multiple-quantum-well lasers," *IEEE Photon. Technol. Lett.*, vol. 12, pp. 969–971, 2000.
[26] G. L. Belenky, R. F. Kazarinov, J. Lopata, S. Luryi, T. Tanbun-Ek, and P. Garbinski, "Direct measurement of the carrier leakage out of the active region in InGaAsP/InP laser heterostructures," *IEEE Trans. Electron Devices*, vol. 42, pp. 215–218, 1995.
[27] H. Yamazaki, A. Tomita, and M. Yamaguchi, "Evidence of nonuniform carrier distribution in multiple quantum well lasers," *Appl. Phys. Lett.*, vol. 71, pp. 767–769, 1997.
[28] W. F. Brinkman and P. A. Lee, "Coulomb effects on the gain spectrum of semiconductors," *Phys. Rev. Lett.*, vol. 31, pp. 237–240, 1973.
[29] W. Bardyszewski and D. Yevick, "Stimulated recombination in highly excited GaAs," *Phys. Rev. B*, vol. 39, pp. 10 839–10 851, 1989.
[30] G. L. Belenky, L. Shterengas, C. L. Reynolds, Jr., M. W. Focht, M. S. Hybertsen, and B. Witzigmann, "Direct measurement of lateral carrier leakage in 1.3 μm InGaAsP MQW CMBH lasers," *IEEE J. Quantum Electron.*, vol. 38, pp. 1276–1281, 2002.
[31] R. Nagarajan, M. Ishikawa, T. Fukushima, J. G. R. S. Geels, and J. E. Bowers, "High speed quantum-well lasers and carrier transport effects," *IEEE J. Quantum Electron.*, vol. 28, pp. 1990–2007, 1992.
[32] N. Tessler and G. Eisenstein, "On carrier injection and gain dynamics in quantum well lasers," *IEEE J. Quantum Electron.*, vol. 29, pp. 1586–1595, 1993.
[33] M. Ishikawa, R. Nagarajan, T. Fukushima, J. G. Wasserbauer, and J. E. Bowers, "Long wavelength high-speed semiconductor lasers with carrier transport effects," *IEEE J. Quantum Electron.*, vol. 28, pp. 2230–2240, 1992.
[34] I. F. Lealman, M. J. Harlow, and S. D. Perrin, "Effect of Zn doping on modulation bandwidth of 1.55 μm InGaAs InGaAsP multiple quantum-well lasers," *Electron. Lett.*, vol. 29, pp. 1197–1198, 1993.
[35] B. Witzigmann and M. S. Hybertsen, "Simulation of temperature dependent modulation response in multi-quantum-well lasers," *SPIE Proc.*, vol. 4646, pp. 313–319, 2002.

Bernd Witzigmann received the M.S. degree in physics from the University of Ulm, Ulm, Germany, in 1996 and the Ph.D. degree (with honors) in technical sciences from the Swiss Federal Institute of Technology (ETH), Zurich, Switzerland, in 2000.

In 2000, he became a postdoctoral Member of Technical Staff in the Semiconductor Photonics Research Department at Bell Laboratories and then Agere Systems (formerly Lucent Technologies), Murray Hill, NJ. In October 2001, he joined the Optical Access and Transport Division of Agere Systems, Alhambra, CA, as a Member of Technical Staff. He has worked on numerical simulation and modeling of semiconductor photonic devices, microwave components, and most recently on the process and device design of modulated laser sources.

Mark S. Hybertsen (M'95) received the B.A. degree in physics from Reed College, Portland, OR, in 1980 and the Ph.D. degree in physics from The University of California at Berkeley in 1986. His thesis research concerned exchange and correlation in semiconductors and insulators.

He joined Bell Laboratories, Murray Hill, NJ, as a postdoctoral Member of Technical Staff in 1986. He was a Member of Technical Staff from 1988 to 1997, conducting a variety of research projects concerning the theory of the electronic properties of materials (bulk semiconductors, semiconductor surfaces and interfaces, cuprates, porous silicon). In recent years, his research has focused on optoelectronic devices. From 1997 to 2001, he supervised the Device and Materials Physics Group in the Semiconductor Photonics Research Department, first at Bell Laboratories and then as a part of Agere Systems (formerly Lucent Technologies). He is presently a Consulting Member of Technical Staff with Agere Systems, Murray Hill, NJ.

Dr. Hybertsen is a Fellow of the American Physical Society and a member of the Optical Society of America and of the Lasers and Electro-Optics Society (LEOS).

C. Lewis Reynolds, Jr., (M'83) received the B.S. degree in physics from the Virginia Military Institute, Lexington, VA, in 1970 and the M.S. and Ph.D. degrees in materials science from the University of Virginia, Charlottesville, in 1972 and 1974, respectively.

He was a Research Associate in physics at the University of Illinois, Urbana, from 1974 to 1977, investigating the low-temperature properties of quantum and amorphous solids. From 1977 to 1980, he was a Senior Project Engineer with Union Carbide Corporation, Indianapolis, IN, working on the deposition of thick-film coatings. Since 1980, he has been a Member of Technical Staff of Bell Laboratories, formerly with AT&T and Lucent Technologies, and most recently with Agere Systems, Breinigsville, PA. During this time, his efforts have been directed toward the growth, characterization, and packaging of AlGaAs and InGaAsP lasers and the growth of heterostructures by molecular beam epitaxy for GaAs integrated circuits. He is currently a member of the Semiconductor Photonics Research Department, working on MOVPE of strained-quantum-well and distributed-feedback InGaAsP lasers, waveguides, and selected area growth. Since 1988, he has also been a Distinguished Member of Technical Staff. He has authored or co-authored more than 100 publications and holds four U.S. patents.

Gregory L. Belenky (M'95–SM'96) received the Ph.D. degree in physics and mathematics from the Institute of Semiconductors, Kiev, Russia, and the Doctor of Physical and Mathematical Sciences degree from the Institute of Physics, Baku, Russia.

He was with AT&T Bell Laboratories, Murray Hill, NJ, before joining the faculty of the State University of New York at Stony Brook in 1995, where he is currently a Professor in the Department of Electrical and Computer Engineering. He has published over 100 papers, several reviews, and filed three U.S. patents dealing with physics of 2-D structures and physics and design of photonic devices. His current research interests include physics of semiconductors and the design and working performance of semiconductor lasers and optoelectronic systems.

Leon Shterengas was born in St. Petersburg, Russia, in 1976. He received the B.A. degree in physics of semiconductors from St. Petersburg State Technical University, St. Petersburg, Russia, in 1998, and the M.S. degree in electrical engineering from the State University of New York at Stony Brook in 1999, where he is currently working toward the Ph.D. degree in electrical engineering. His research is focused on the design, development, and characterization of semiconductor lasers.

Gleb E. Shtengel was born in Novosibirsk, Russia, in 1968. He received the M.Sc.degree in physics from St. Petersburg State Technical University, St. Petersburg, Russia, in 1991, and the Ph.D. degree in physics from Stevens Institute of Technology, Hoboken, NJ, in 1996.

In 1991 he joined the A. F. Ioffe Physical-Technical Institute, St. Petersburg, Russia, where he studied the physics of AlGaAs lasers. In 1993, he was a Visiting Researcher at Colorado State University, Fort Collins, where he worked on vertical-cavity surface-emitting lasers. In 1994, he joined AT&T Bell Laboratories (formerly Lucent Technologies), Breinigsville, PA. There, he worked on the design of semiconductor lasers, modulators and other components for fiber telecommunication systems. In 2000, he joined YAFO Networks Inc., Hanover, MD, to work on polarization mode dispersion compensation. In 2001, he joined Kodeos Communications, South Plainfield, NJ. He has coauthored over 40 papers and conference talks and holds five patents.